Report No. 1

AN ANALOG EXPERIMENT ON TURBULENT LIQUID METAL HEAT TRANSFER IN THE ENTRANCE REGION OF NON CIRCULAR DUCTS

by

J. T. Pearson, Jr.

and

T. F. Irvine, Jr.

MARCH, 1963

AN ANALOG EXPERIMENT ON TURBULENT LIQUID METAL HEAT TRANSFER IN THE ENTRANCE REGION OF NONCIRCULAR DUCTS

by

J. T. Pearson, Jr.*

and

T. F. Irvine, Jr.**

Abstract

An electric analogue made of Teledeltos paper, dielectric sheets and metal foil was utilized for the solution of the Fourier equation in two dimensions.

The analogue was used to determine the steady state slug flow wall temperature distributions in the entrance region of ducts having a variety of noncircular shapes. These temperature distributions are a limiting case of turbulent liquid metal duct flow. The boundary condition for the fluid was one of constant heat input per unit of duct wall area and the cross sectional shapes considered were circles, parallel plates, equilateral triangles, squares, pentagons, hexagons and octagons.

In the case of the parallel plates and circles where analytic solutions were available, the experimental results showed satisfactory agreement.

---

*Instructor, Thermal Sciences Department, College of Engineering, State University of New York at Stony Brook, New York

**Professor and Dean, College of Engineering, State University of New York at Stony Brook, New York

INTRODUCTION

Weight and space limitations in many present day heat exchangers present critical problems in the selection of suitable passage shapes and frequently dictate passages of noncircular cross section. Often the passage lengths are so short that the temperature and velocity profiles are not fully developed before the fluid exits from the passage. Thus, for many compact exchangers, the thermal and hydraulic entrance region occupies a major portion of the passage length.

For fully developed turbulent flow of a liquid metal in circular ducts it has been found by Lyon[1], Claiborne[2] and others that the heat transfer performance may be estimated by an appropriate combination of the separate contributions due to molecular conduction and turbulent exchange. Since the velocity profile in turbulent flow approximates a slug flow profile, it is reasoned that the convective heat transfer due to molecular conduction may be obtained from the energy equation utilizing the actual boundary conditions but assuming a constant velocity distribution. The application of this approach to noncircular duct heat transfer was treated by Hartnett and Irvine[3].

The above authors in the same paper also discussed the various boundary conditions which may be encountered in noncircular duct heat transfer. In particular they pointed out that if the heat flux is specified, the peripheral wall temperature distribution is of greatest interest since structural considerations normally dictate a maximum possible operating temperature. Thus, the wall temperature distribution predicted by the slug flow analysis may be taken as a limiting case in turbulent flow. Any turbulent contribution will have a mitigating effect on the slug flow temperature distribution.

The purpose of the present paper is to provide these slug flow temperature distributions in the entrance region of ducts having a variety of cross sectional shapes. For design purposes these distributions represent extreme cases but should be useful since their utilization will produce conservative designs, which approach true design conditions at low Reynolds numbers in turbulent flow.

It is also of interest to note that the steady state slug flow convection problem is the same as the problem of unsteady state heat conduction in a two dimensional solid with the same cross sectional shape and the same boundary conditions. The solutions reported here for all of the shapes except the parallel plates and the circles have not been available before.

Governing Equations and Basis for Electrical Analogy

Consider the entrance region of a duct with a constant cross sectional shape as shown in Figure 1. A fluid enters the duct at a constant temperature T_o and flows through the duct with a constant velocity w. The coordinate system is selected so that the z axis pierces the centroid of the duct's cross section and the origin is at the duct's entrance. For constant fluid properties, incompressible flow, negligible viscous energy dissipation and axial heat conduction, the steady energy equation can be written as

$$\frac{\partial^2 T}{\partial x^2} + \frac{\partial^2 T}{\partial y^2} = \frac{w}{\alpha} \frac{\partial T}{\partial z} . \tag{1}$$

Under the constant heat flux condition, the boundary conditions for Equation (1) are

$$\frac{\partial T}{\partial n} = - \frac{q_w}{k} = \text{const. on } \Gamma, \tag{2}$$

$$T(x, y, 0) = T_o = \text{const.}, \tag{3}$$

where n is the direction perpendicular to the duct's surface and $\sigma = \sigma(x, y)$ is the inside surface of the duct. If Equation (1) and its boundary conditions are made dimensionless by selecting the following variables:

$$\Theta = \frac{T - T_o}{4q_w d_h/k}, \qquad Z = \frac{z}{d_h RePr},$$

$$X = \frac{x}{d_h}, \qquad Y = \frac{y}{d_h}, \qquad N = \frac{n}{d_h},$$

Equation (1) becomes

$$\frac{\partial^2\Theta}{\partial X^2} + \frac{\partial^2\Theta}{\partial Y^2} = \frac{\partial\Theta}{\partial Z} \tag{4}$$

and boundary conditions (2) and (3) become

$$\frac{\partial\Theta}{\partial N} = -\frac{1}{4} \quad \text{on } \Sigma, \tag{5}$$

$$\Theta(X, Y, 0) = 0, \tag{6}$$

where $\Sigma = \Sigma(X, Y)$ is the dimesnionless inside surface of the duct.

The bulk temperature of the fluid is found by performing an energy balance on an increment of fluid

$$dT_b = \frac{q_w P}{wA\rho c}\, dz. \tag{7}$$

Integrating from $T_b = T_o$, $z = 0$ to $T_b = T_b$, $z = z$ yields

$$\int_{T_o}^{T_b} dT_b = \int_0^z \frac{q_w P}{wA\rho c}\, dz \tag{8}$$

or

$$T_b = T_o + \frac{4q_w \mathcal{Z}}{wkd_h}. \tag{9}$$

Making this equation dimensionless gives

$$\Theta_b = Z. \tag{10}$$

Now consider the electrical model described by Fatt[4] which is composed of a thin dielectric sheet sandwiched between an electrically conducting resistance sheet and a sheet of metal foil as shown in Figure 2. The model boundary is the curve $\sigma^* = \sigma^*(x^*, y^*)$ which has the same shape as the duct cross section $\sigma(x,y)$. The coordinate system (x^*, y^*) is oriented so that the origin is at the centroid of the curve σ^* and the (x^*, y^*) plane is in the plane of the model. An electric current is allowed to flow into the model at the curve σ^* and the circuit is completed by gounding the metal foil. If the resistivity of the resistance sheet and the thickness of the dielectric are uniform over the model, the governing differential equation is

$$\frac{\partial^2 E}{\partial x^{*2}} + \frac{\partial^2 E}{\partial y^{*2}} = RC \frac{\partial E}{\partial t}. \tag{11}$$

If the electrical current flowing into the model is constant per unit length of σ^* after a certain time $t = 0$ and if the entire model is at a uniform voltage E_o until $t = 0$ the boundary conditions of equation (11) are

$$\frac{\partial E}{\partial n^*} = -Ri_w = \text{const. on } \sigma^*, \tag{12}$$

$$E(x^*, y^*, 0) = E_o = \text{const.}, \tag{13}$$

where n^* is the direction perpendicular to the boundary σ^*. Now if these equations are normalized by selected the following dimensionless variables:

$$\Theta^* = \frac{E - E_o}{4i_w d_h^* R}, \qquad Z^* = \frac{t}{d_h^{*2} RC},$$

$$X^* = \frac{x^*}{d_h^*}, \qquad Y^* = \frac{y^*}{d_h^*}, \qquad N^* = \frac{n^*}{d_h^*},$$

Equation (11) becomes

$$\frac{\partial^2 \Theta^*}{\partial X^{*2}} + \frac{\partial^2 \Theta^*}{\partial Y^{*2}} = \frac{\partial \Theta^*}{\partial Z^*} \tag{14}$$

and boundary conditions (12) and (13) become

$$\frac{\partial \Theta^*}{\partial N^*} = -\frac{1}{4} \quad \text{on} \quad \sum^*, \tag{15}$$

$$\Theta^* (X^*, Y^*, 0) = 0 \tag{16}$$

where $\sum^* = \sum^* (X^*, Y^*)$ is the dimensionless expression for curve σ^*.

The bulk voltage E_b of the electrical model may be found by performing an energy balance on the model.

$$dE_b = \frac{i_w P^*}{A^* C} \, dt. \tag{17}$$

Integrating from E_o to E_b and from time zero to t gives

$$\int_{E_o}^{E_b} dE_b = \int_0^t \frac{i_w P^*}{A^* C} \, dt \tag{18}$$

or

$$E_b = E_o \frac{4 i_w t}{C d_n^*} \tag{19}$$

or in dimensionless form

$$\Theta^*_b = Z^*. \tag{20}$$

Comparing Equation (4) and its boundary conditions [Equations (5) and (6)] with Equation (14) and its boundary conditions [Equations (15) and (16)] it is seen that the two systems of equations are identical in form so that the solution of one system is the solution of the other. The constant heat input boundary condition is replaced by a constant current input in the electric model. This is the basis of the present study.

Experimental Procedure

The apparatus consists of the components shown in Figure 3. In order to approximate a constant electrical current flow into the model at the boundary, it was necessary to divide the current input into a finite number of constant current inputs along the boundary. The method which gave the most satisfactory

results is illustrated in Figure 4.

Type L Teledeltos paper which had a resistivity of about 1,400 ohms per square was selected as the resistance sheet. The resistivity of this paper was linear within 2 percent in any particular direction but the resistivity across the sheet was approximately 10 percent greater than the resistivity along the sheet. In order to make the resistivity of the models more nearly uniform in all directions the models were made of two layers of resistance paper cut so that the direction across the sheet on one half of the model corresponded to the direction along the sheet on the other half. With the conducting sides of the paper touching, the resistivity of the models was approximately 700 ohms per square.

In order to increase the capacitance of the model, sheets of dielectric and metal foil were placed on each side of the resistance model as shown in Figure 4. This made the capactiance of the model approximately 1,000 pfd. per square inch.

Rather than measure all the parameters required to evaluate the dimensionless voltage Θ^* and the dimensionless time Z^*, an auxiliary model, as shown in Figure 4, was constructed from resistance paper immediately adjacent to that from which the primary model was cut. Here again the auxiliary model was cut from two pieces of resistance paper oriented at right angles to each other.

By analysis it is found that the voltage measured at the tabs of the auxiliary model is

$$E_{aux} = 4\, i_w R$$

Another helpful measurement can be made on the model itself. The slope of voltage vs. time curve approaches a constant value as t increases. By analysis it is found that

$$\left.\frac{dE}{dt}\right|_{t \gg 0} = \frac{4 i_w}{C d_n^*} \qquad (21)$$

Applying this information to the dimensionless variables yields

$$Q^* = \frac{E - E_o}{4\, i_w R d_h^*} = \frac{E - E_o}{E_{aux} d_h^*} \qquad (22)$$

and

$$Z^* = \frac{t}{d_h^{*2} RC} = \frac{t}{4 i_w R d_h^*} \cdot \left.\frac{dE}{dt}\right| \quad t \gg o = \frac{t}{E_{aux} d_h^*} \cdot \left.\frac{dE}{dt}\right| \quad t > o \qquad (23)$$

Therefore, it is seen that Q^* and Z^* can be determined from measurements of E_o, E, t, d_h^*, E_{aux} and dE/dt.

The model holder, which is shown in Figure 3, was constructed so that it shielded the model and input resistors from stray electrical effects without creating excessive stray capacitance. The rubber diaphragm presses the model and auxiliary model together with a uniform force of about seven pounds per square inch when the pressure reservoir is pressurized by use of a bicycle pump. The cover shield has 40 3/16 inch diameter holes drilled along its base so that the base of each input resistor is accessible to the probe from the oscilloscope. A shielded lead was attached to the bus bar and exited through the end of the cover shield. The lead is three inches long and terminates with a banana plug which is inserted into the 600 ohm 55 volt output socket of the square wave generator. Greater details on the preparation of the model and the technique of data taking are to be found in a thesis study by Pearson[5].

Comparison of Analogue Solutions with Analytical Solutions

Analytical solutions for slug flow wall temperature distributions in circular tubes and between parallel plates with constant wall heat flux may be obtained from unsteady convection solutions presented by Siegel[6]. Transforming these solutions into the dimensionless variables selected in this investigation yields

$$Q_w = Z + \frac{1}{48} - \frac{1}{8\pi^2} \sum_{n=1}^{\infty} \frac{e^{-16n^2\pi^2 Z}}{n^2} \qquad (24)$$

for parallel plates and

$$\theta_w = Z \frac{1}{32} - \frac{1}{4} \sum_{n=1}^{\infty} \frac{e^{-4B_n^2 Z}}{B_n^2} \qquad (25)$$

for circular ducts where B_n are the positive roots of $J_1(B) = 0$.

The dimensionless wall temperature θ_w has been calculated for various Z locations along the tube and parallel plate surfaces by Cess[7] employing up to 35 terms of the series. These results are shown in Figures 5 and 6 as solid lines. Experimental data obtained on the apparatus described previously is also presented in these figures. It is seen that the agreement is satisfactory.

Solutions for Equilateral Polygons

Using the same experimental techniques, measurements were made on the other geometries. The data for the equilateral triangle are shown in Figures 7 and 8. Figure 7 illustrates the dimensionless wall temperature variation at two wall locations as it changes down the duct. Figure 8 gives the peripheral wall temperature distributions at various distances from the entrance.

The dashed lines on the two figures are the fully-developed solutions as given by Claiborne[2]. Again the agreement is seen to be satisfactory. It should be pointed out that Figure 8 is a cross-plot of a series of experimental curves similar to Figure 7.

Figures 9, 10, 11 and 12 show the wall temperature distributions for squares, pentagons, hexagons, and octagons respectively. The dashed curves again represent the asymptotic solutions far from the duct entrance. These asymptotic solutions were obtained from the solution for an n sided equilateral polygon,

$$\theta_w = Z + \frac{1}{16}\left\{\left[\left(\frac{X}{L}\right)^2 - \frac{1}{6}\right] \tan^2 \frac{\pi}{n} + \frac{1}{2}\right\} \qquad (26)$$

which to the authors' knowledge has not been previously published.

Summary

Entrance wall temperature distributions are presented for a number of noncircular ducts. These distributions are limiting cases for the turbulent flow of a liquid metal in the entrance regions of these ducts. The data were obtained by an analogue technique which proved to be simple and accurate.

NOMENCLATURE

A	-cross sectional area of duct
A^*	-surface area of electrical model
B_n	-positive roots of $J_1(B) = 0$
c	-specific heat
C	-capacitance of model per unit area
d_h	-hydraulic diameter of duct
d_h^*	-hydraulic diameter of electrical model
E	-voltage at any point on electrical model
E_{aux}	-voltage at tab of auxiliary model
i_w	-electrical current flowing into model per unit length of boundary
J_1	-Bessel function of first order
k	-thermal conductivity
n	-distance normal to duct wall
n^*	-distance normal to electrical model boundary
N	-dimensionless distance along normal to duct wall, $N = n/d_h$
N^*	-dimensionless distance along normal to electrical model boundary, $N^* = n^*/d_h^*$
P	-perimeter of duct
P^*	-perimeter of electrical model
Pr	-Prandtl number, $Pr = \nu/\alpha$
q_w	-heat flux into fluid per unit area of duct wall
R	-resistivity of resistance sheet in resistance per square
Re	-Reynolds number, $Re = wd_h/\nu$
t	-time
T	-temperature
w	-fluid velocity in z direction

x, y, z -coordinate axes in thermal system

x^*, y^* -coordinate axes of electrical analogue model

X, Y, Z -dimensionless coordinates of thermal system, $X = x/d_h$, $Y = y/d_h$, $Z = z/d_h RePr$

X^*, Y^*, Z^* -dimensionless coordinates of electrical analogue model, $X^* = x^*/d_h^*$, $Y^* = y^*/d_h^*$, $Z^* = t/d_h^{*2}RC$

α -thermal diffusivity $\alpha = \frac{k}{\rho c}$

θ -dimensionless temperature, $\theta = (T - T_o)/4q_w d_h/k$

θ^* -dimensionless voltage, $\theta^* = (E - E_o)/4i_w d_h^* R$

ρ -density

σ -the surface representing the inside surface of the duct

σ^* -the curve respresenting the boundary of the electrical model

$\sum$ -the dimensionless form of the surface σ

$\sum^*$ -the dimensionless form of the curve σ^*

Subscripts

b -bulk or average

w -wall or boundary

o -condition at $z = 0$ or $t = 0$

BIBLICGRAPHY

1. Lycn, R. N., "Forced Convection Heat Transfer Theory and Experiments with Liquid Metals", Cak Ridge National Laboratory Report 361 (1949).

2. Claiborne, H. C., "Heat Transfer in Noncircular Ducts", Cak Ridge National Laboratory Report 985 (1951).

3. Hartnett, J. P. and Irvine, T. F., Jr., "Nusselt values for Estimating Turbulent Liquid Metal Heat Transfer in Noncircular Ducts", A.I.Ch.E. Jour., vol. 3 (1957), p. 313.

4. Fatt, I., "A new Electric Analogue Mcdel for Nonsteady State Flow Problems", A.I.Ch.E. Jour., vol. 4 (1958), p. 49.

5. Pearson, J. T., Jr., "Slug Flow Heat Transfer in the Entrance Region of Noncircular Ducts by an Analogue Technique", M. S. Thesis, North Carolina State College (1961).

6. Siegel, R., "Transient Heat Transfer for Laminar Slug Flow in Ducts", Trans. A.S.M.E., vol. 81 (1959), p. 140.

7. Cess, R. D., personal ccmmunication.

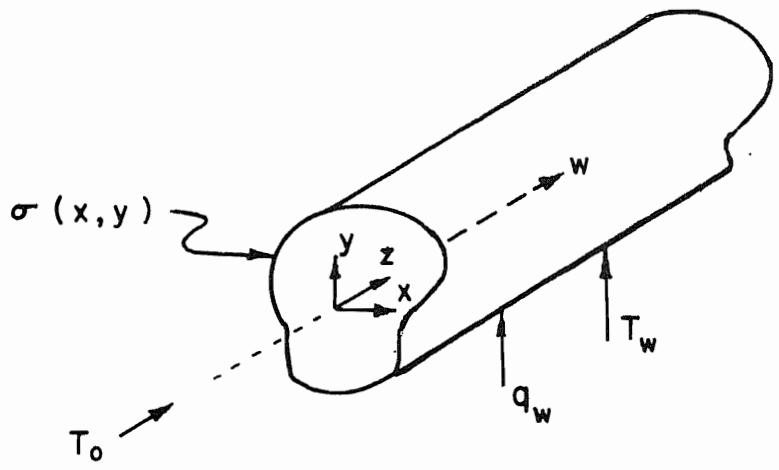

Figure 1. Noncircular duct with arbitrary cross sectional shape

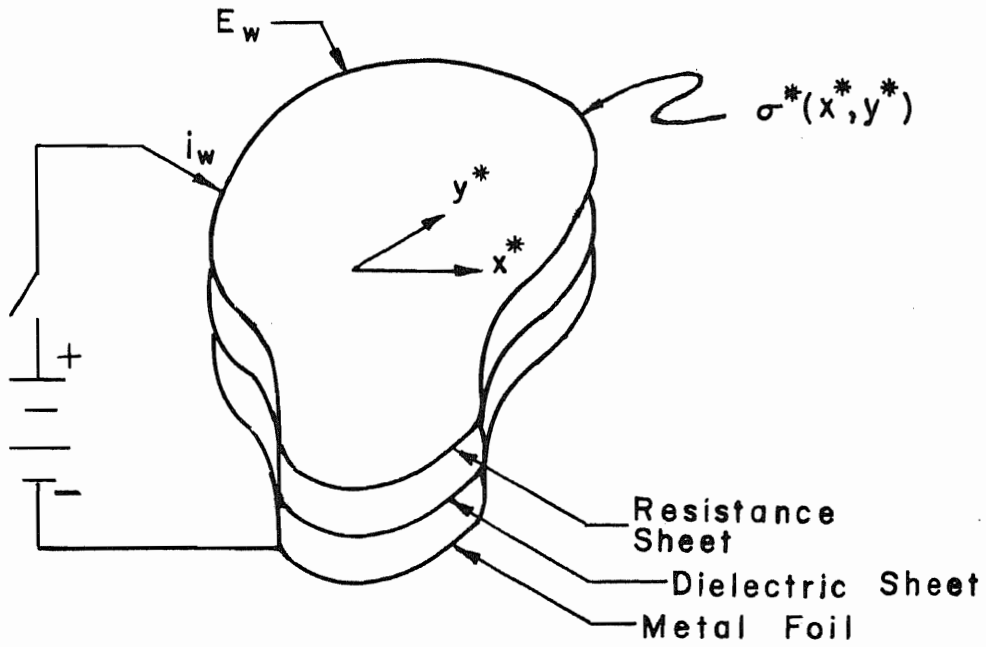

Figure 2. Resistance-capacitance electric analogue model with same cross sectional shape as duct

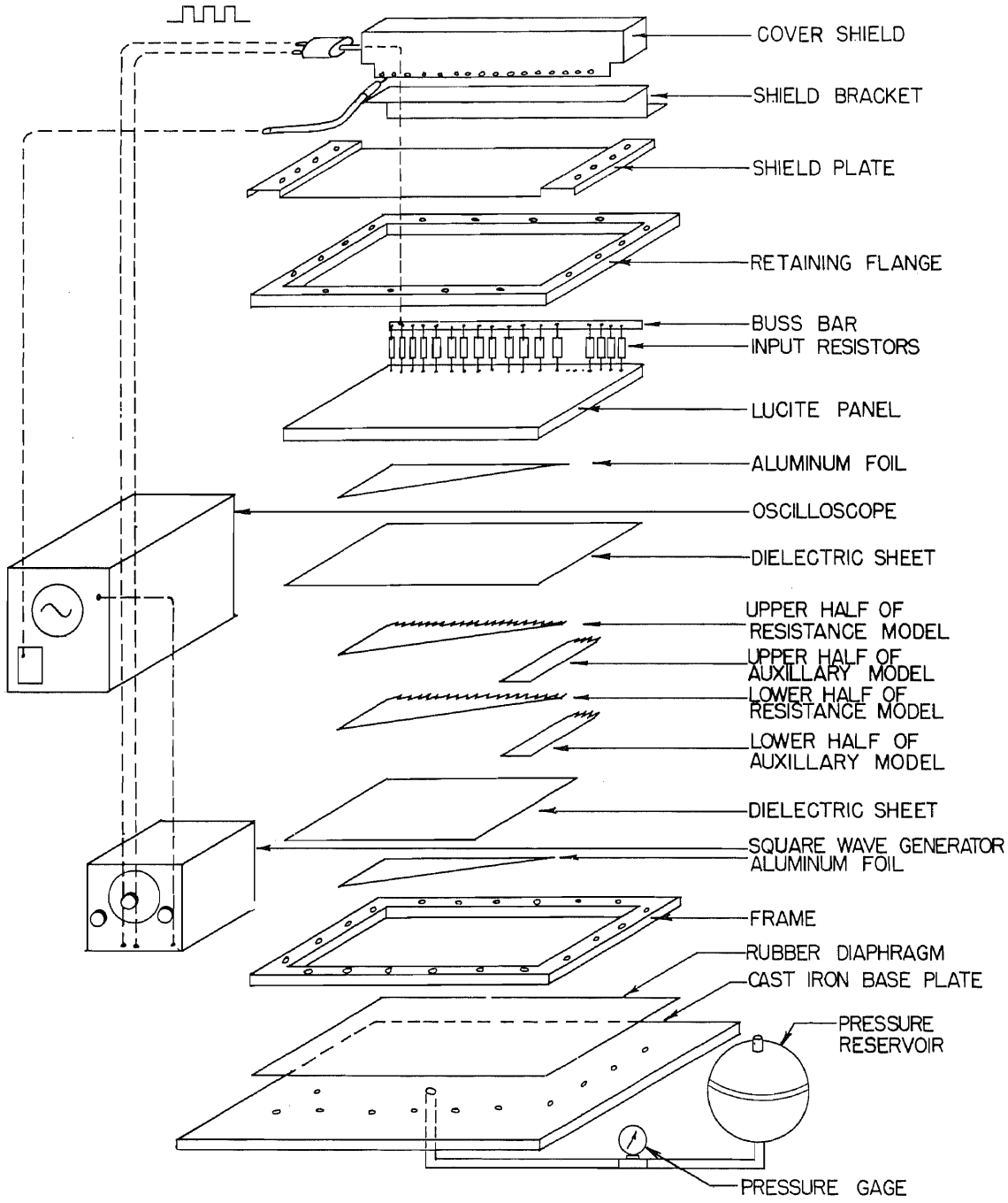

Figure 3. Basic components of apparatus

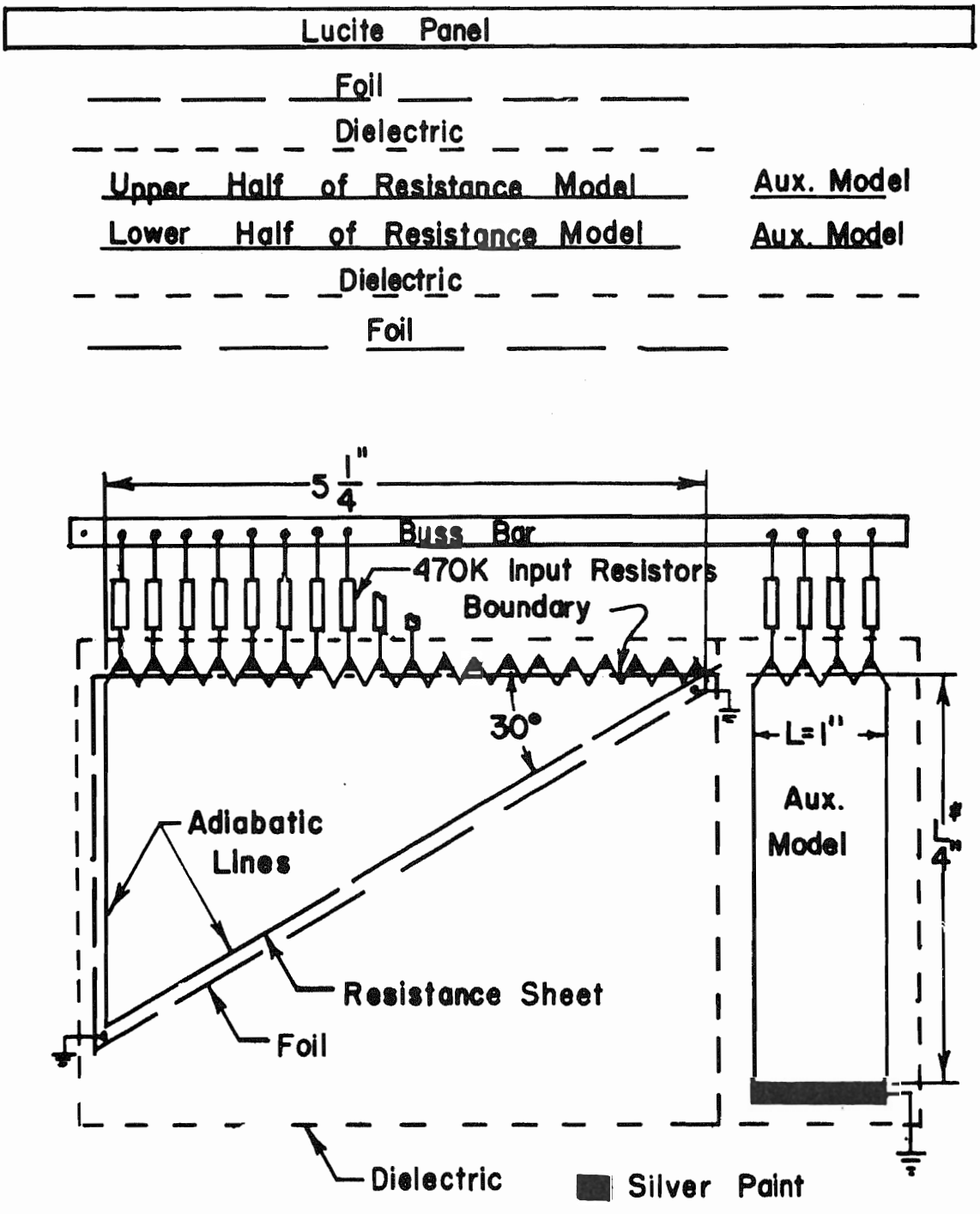

Figure 4. Model and auxiliary model used in solution of equilateral triangular duct geometry showing how models were constructed and positioned

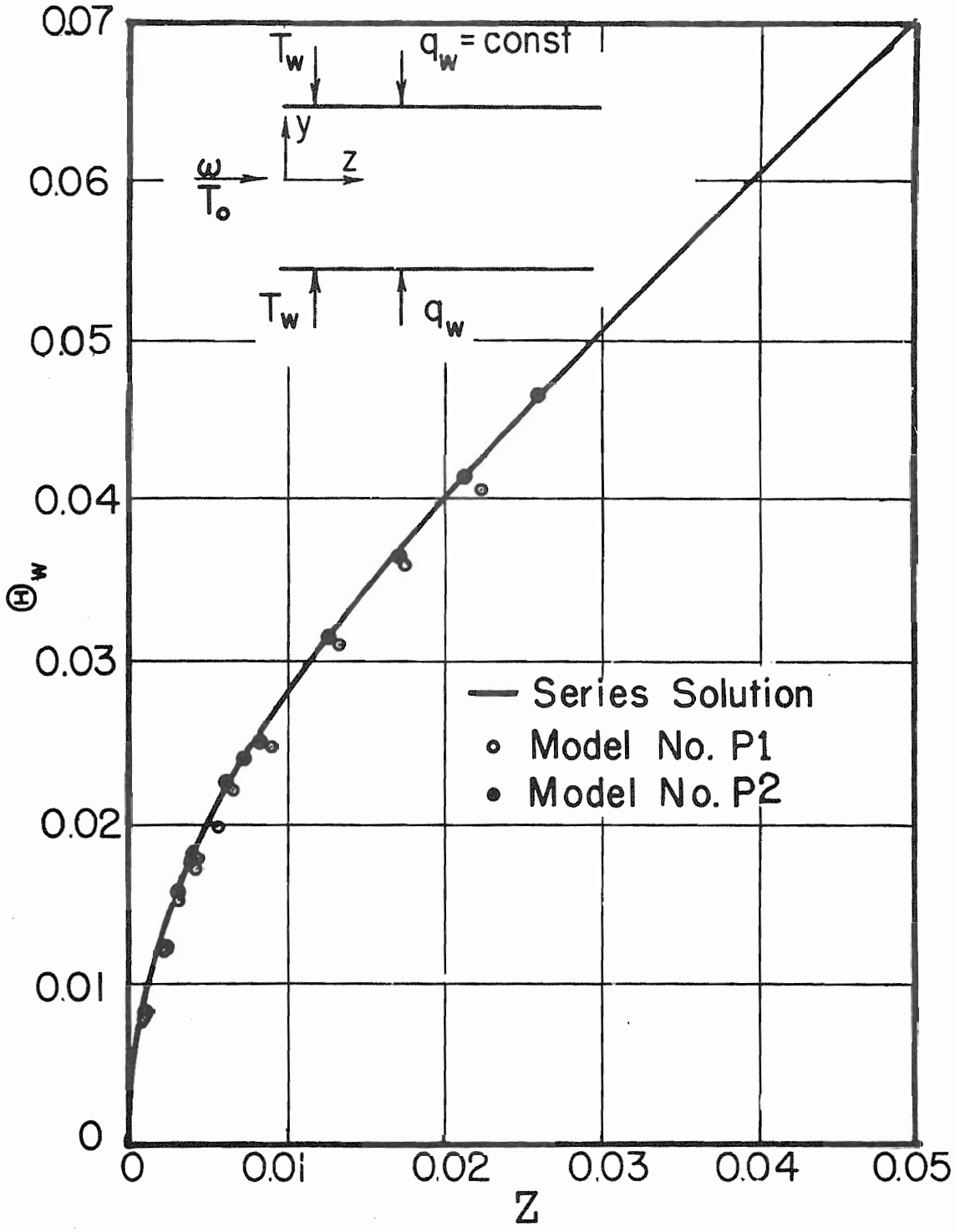

Figure 5. Variation of dimensionless wall temperature for slug flow between parallel plates with constant heat flux at each plate

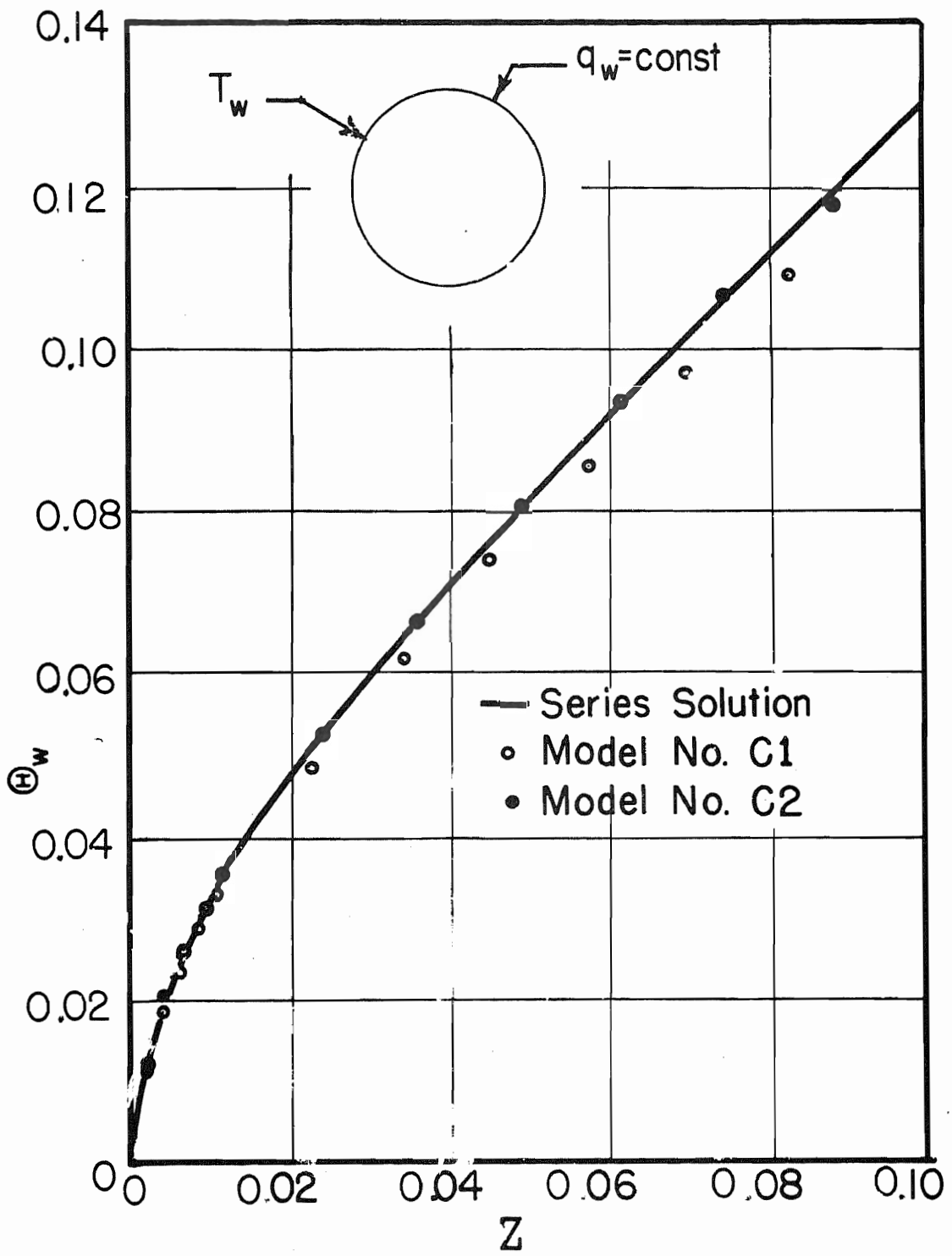

Figure 6. Variation of dimensionless wall temperature for slug flow through a circular duct with constant heat flux at the wall

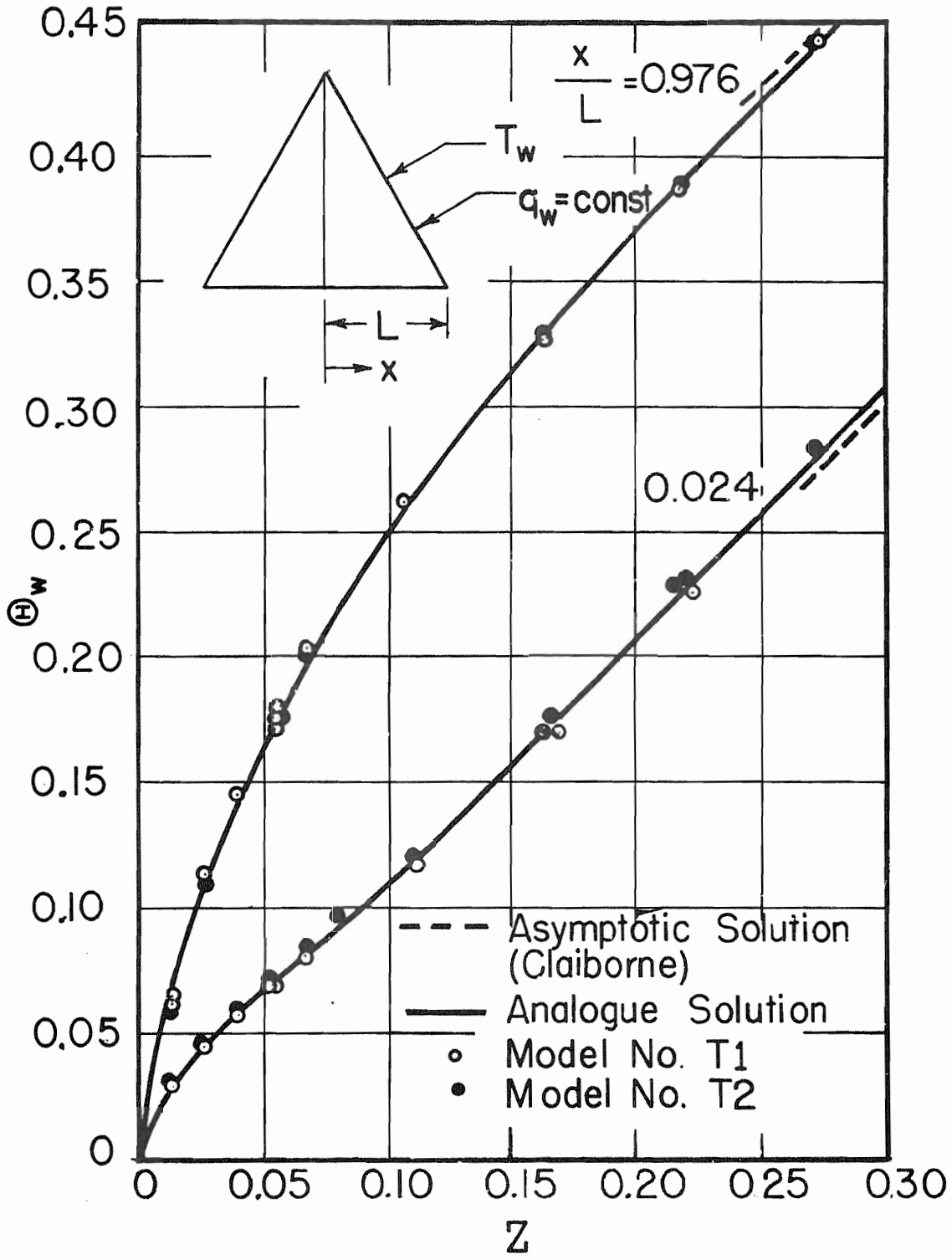

Figure 7. Variation of dimensionless wall temperature for slug flow through an equilateral triangular duct with constant heat flux at the wall

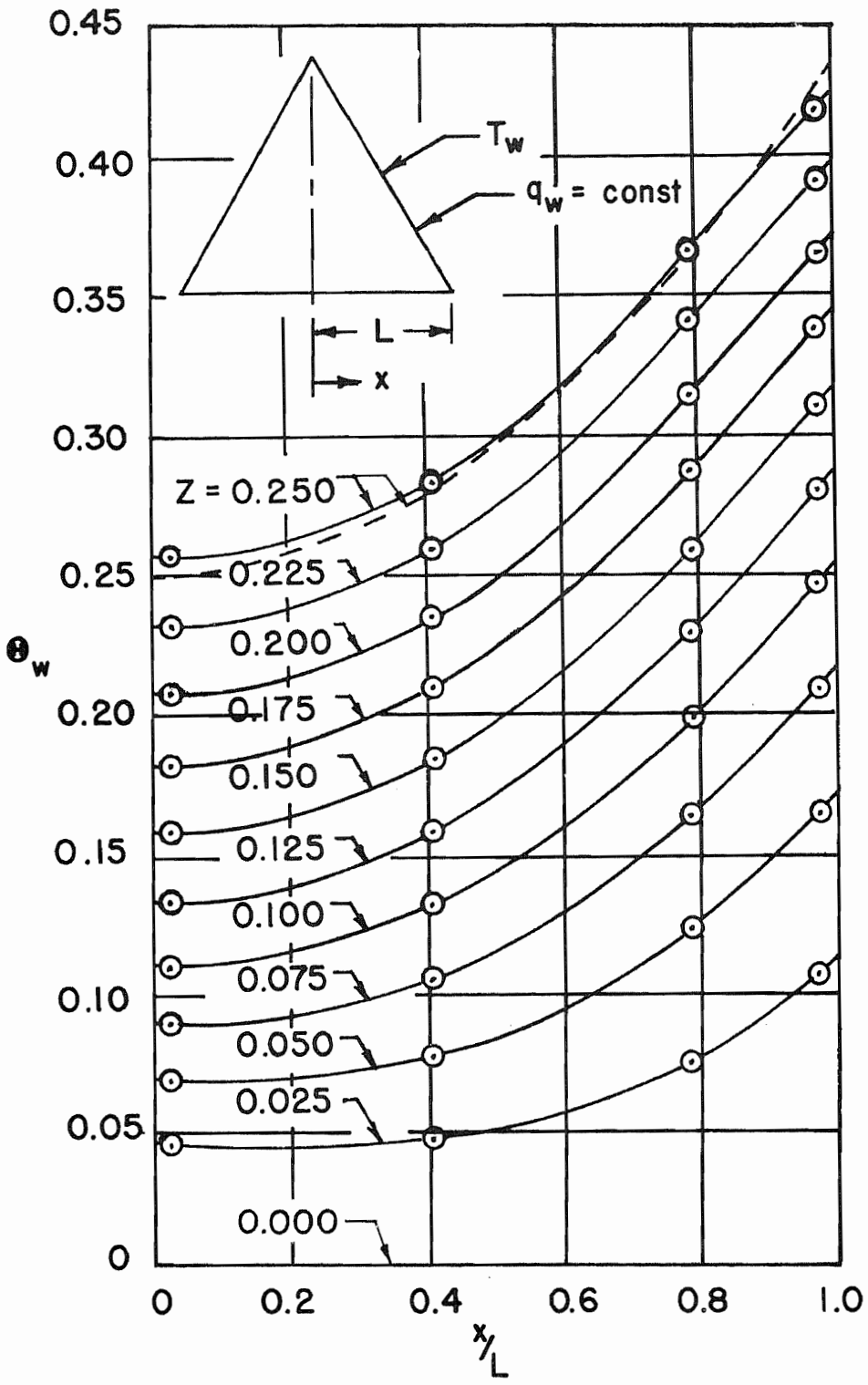

Figure 8. Distribution of dimensionless wall temperature for slug flow through an equilateral triangular duct with constant heat flux at the wall

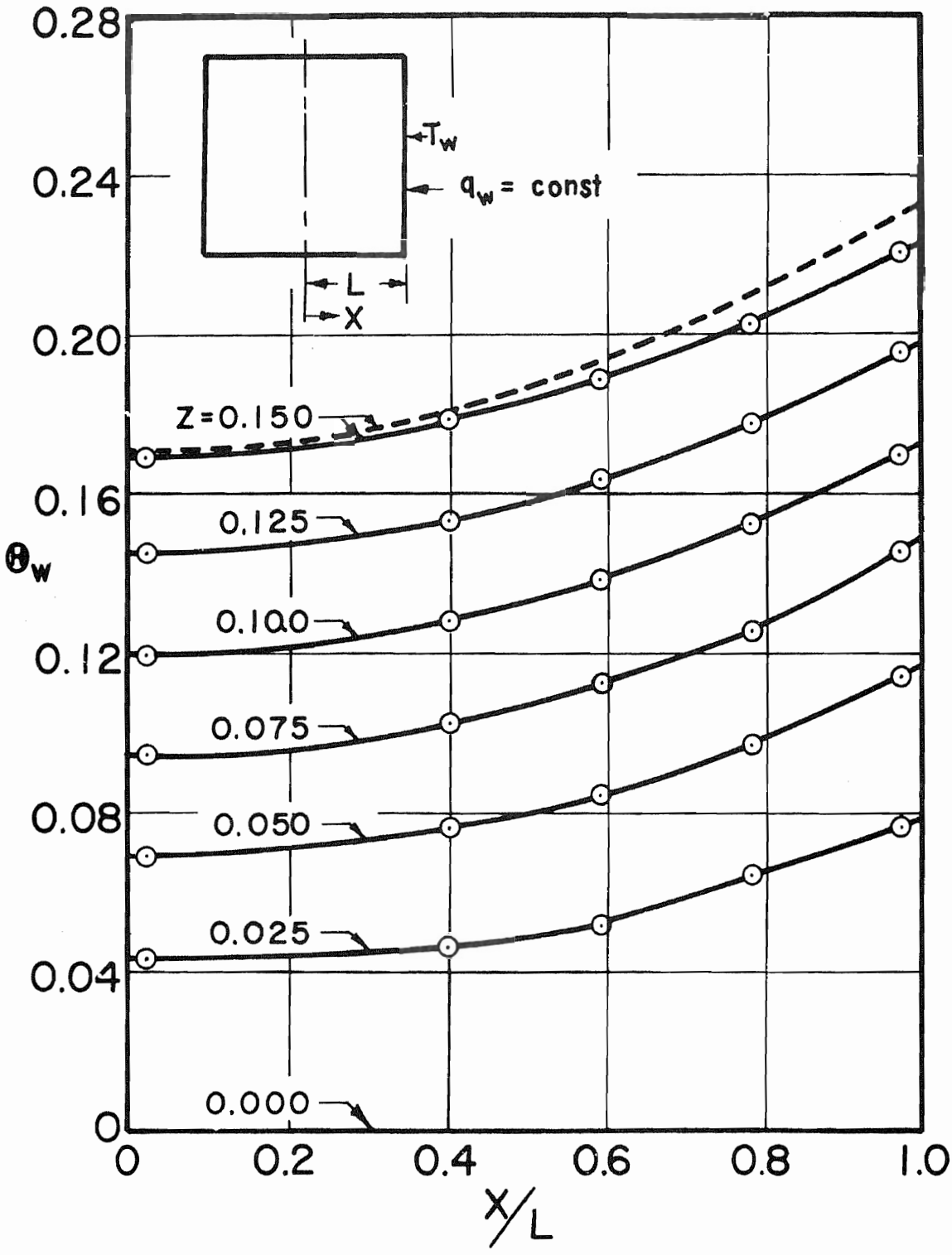

Figure 9. Distribution of dimensionless wall temperature for slug flow through a square duct with constant heat flux at the wall

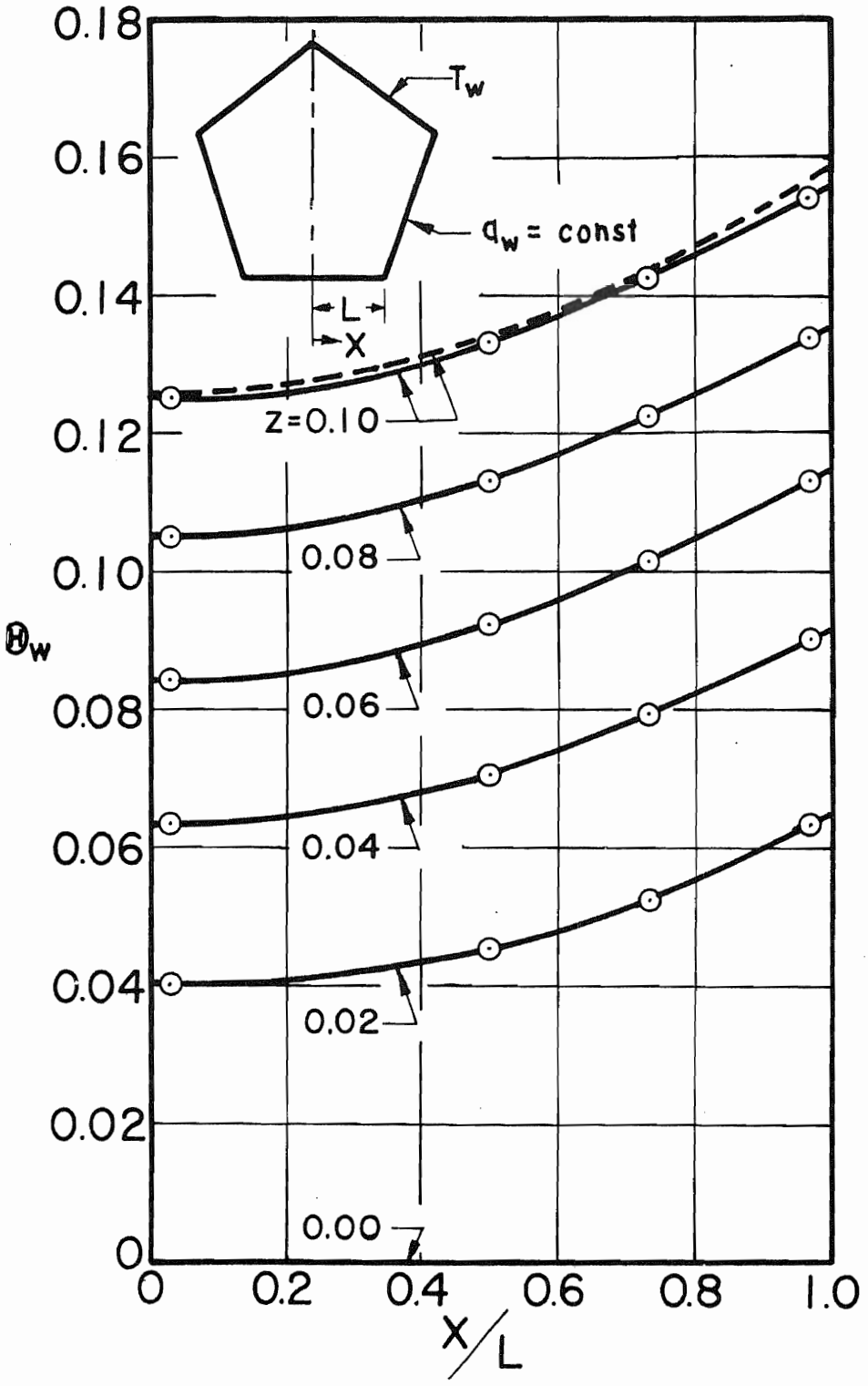

Figure 10, Distribution of dimensionless wall temperature for slug flow through an equilateral pentagonal duct with constant heat flux at the wall

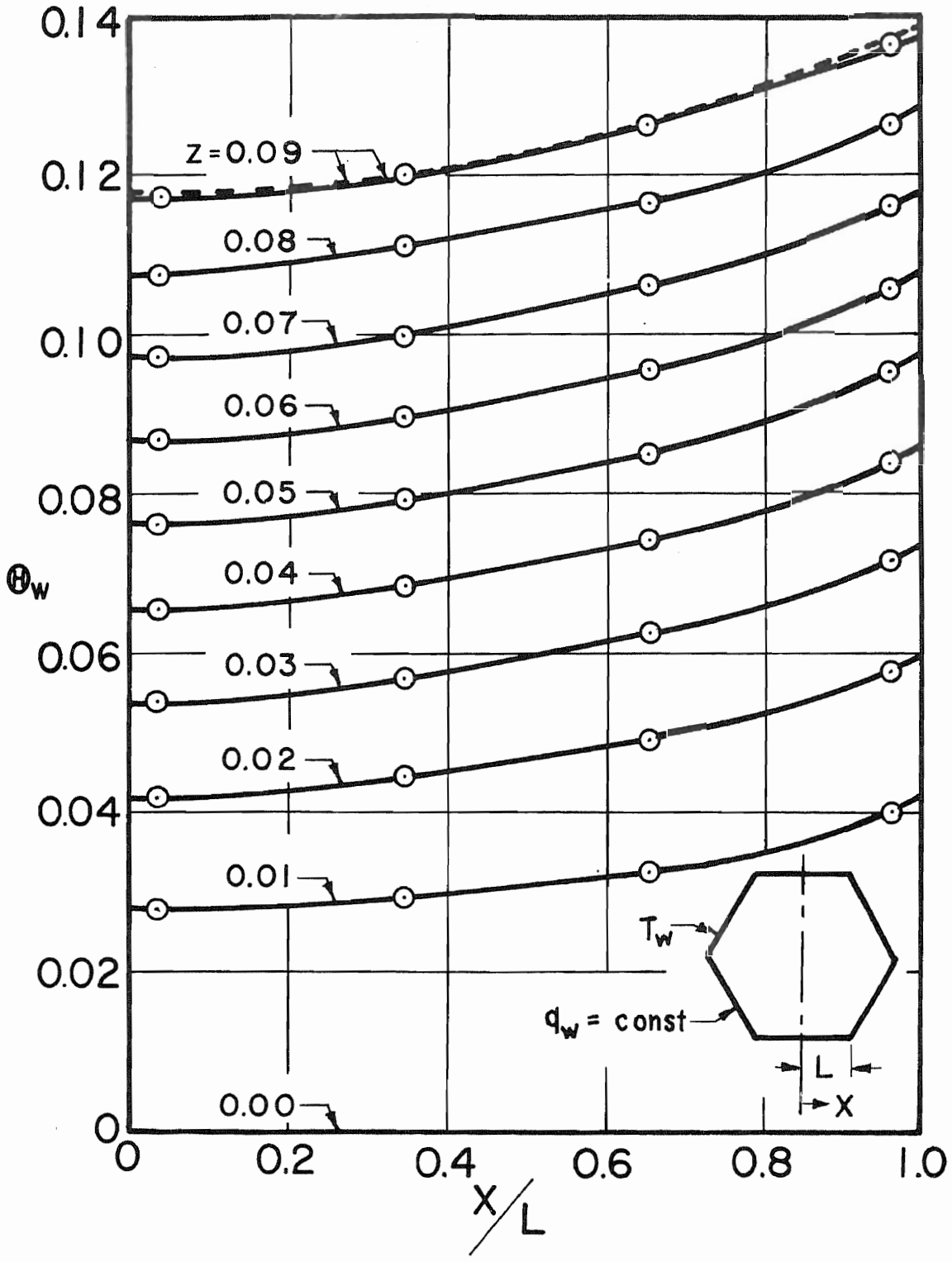

Figure 11. Distribution of dimensionless wall temperature for slug flow through an equilateral hexagonal duct with constant heat flux at the wall

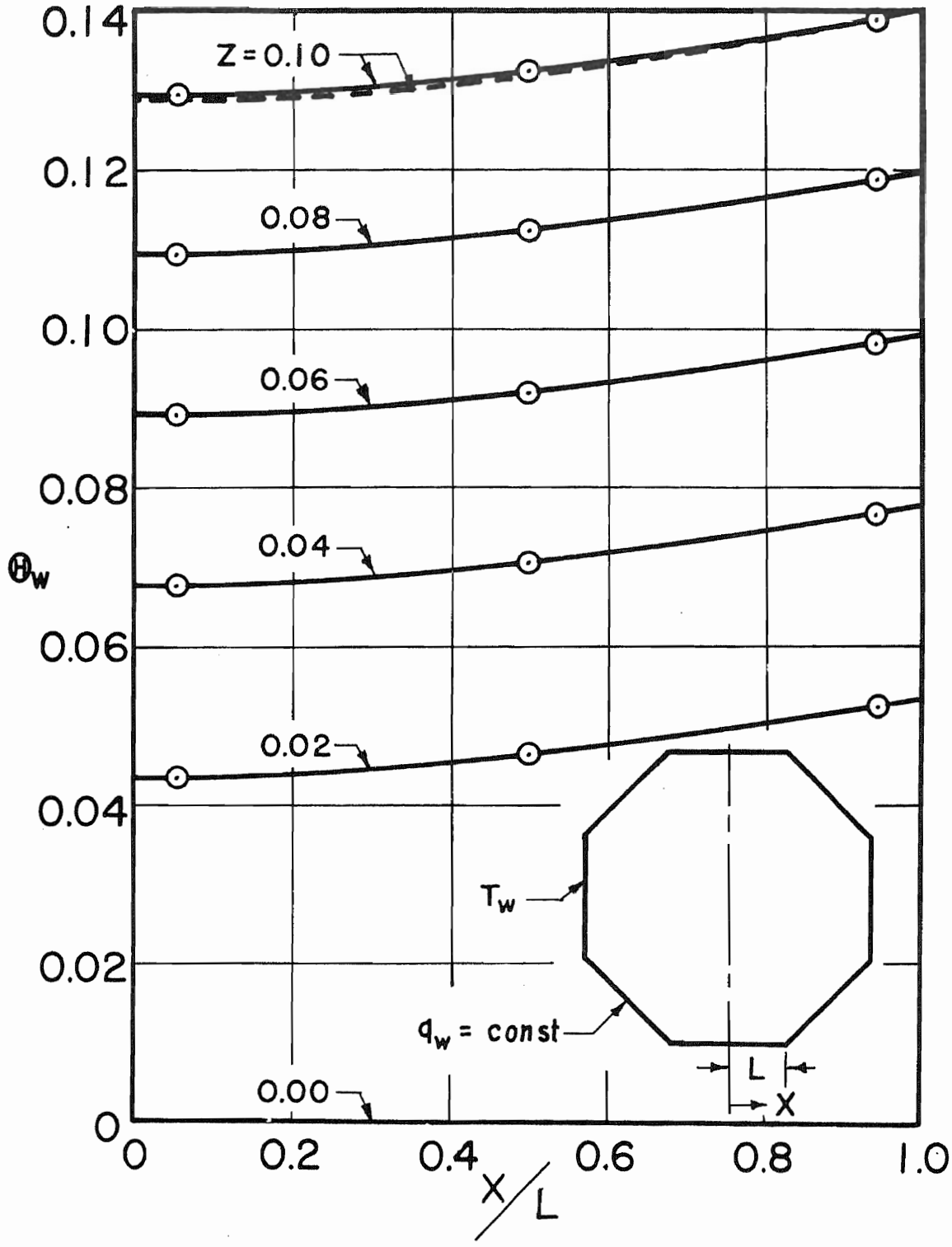

Figure 12. Distribution of dimensionless wall temperature for slug flow through an equilateral octagonal duct with constant heat flux at the wall